Environmental Science & Technology

Article

pubs.acs.org/est

Au Nanoparticles Decorated TiO_2 Nanotube Arrays as a Recyclable Sensor for Photoenhanced Electrochemical Detection of Bisphenol A

Liangsheng Hu,[†,∥] Chi-Chun Fong,[†,‡,⊥] Xuming Zhang,[§] Leo Lai Chan,[†,⊥] Paul K. S. Lam,[⊥] Paul K. Chu,[§] Kwok-Yin Wong,[∥] and Mengsu Yang*[,†,‡,⊥]

[†]Department of Biomedical Sciences, City University of Hong Kong, 83 Tat Chee Avenue, Kowloon, Hong Kong

[‡]Key Laboratory of Biochip Technology, Shenzhen Biotech and Health Centre, City University of Hong Kong, Shenzhen 518057, People's Republic of China

[⊥]State Key Laboratory in Marine Pollution, City University of Hong Kong, 83 Tat Chee Avenue, Kowloon, Hong Kong

[§]Department of Physics and Materials Science, City University of Hong Kong, 83 Tat Chee Avenue, Kowloon, Hong Kong

[∥]Department of Applied Biology and Chemical Technology, and the State Key Laboratory of Chirosciences, The Hong Kong Polytechnic University, Hung Hom, Kowloon, Hong Kong

Supporting Information

ABSTRACT: A photorefreshable and photoenhanced electrochemical sensing platform for bisphenol A (BPA) detection based on Au nanoparticles (NPs) decorated carbon doped TiO_2 nanotube arrays (TiO_2/Au NTAs) is described. The TiO_2/Au NTAs were prepared by quick annealing of anodized nanotubes in argon, followed by controllable electrodeposition of Au NPs. The decoration of Au NPs not only improved photoelectrochemical behavior but also enhanced electrocatalytic activities of the resulted hybrid NTAs. Meanwhile, the high photocatalytic activity of the NTAs allowed the electrode to be readily renewed without damaging the microstructures and surface states after a short UV treatment. The electrochemical detection of BPA on TiO_2/Au NTAs electrode was significantly improved under UV irradiation as the electrode could provide fresh reaction surface continuously and the further increased photocurrent resulting from the improved separation efficiency of the photogenerated electron−hole pairs derived from the consumption of holes by BPA. The results showed that the refreshable TiO_2/Au NTAs electrode is a promising sensor for long-term BPA monitoring with the detection limit (S/N = 3) of 6.2 nM and the sensitivity of 2.8 $\mu A \cdot \mu M^{-1} \cdot cm^{-2}$.

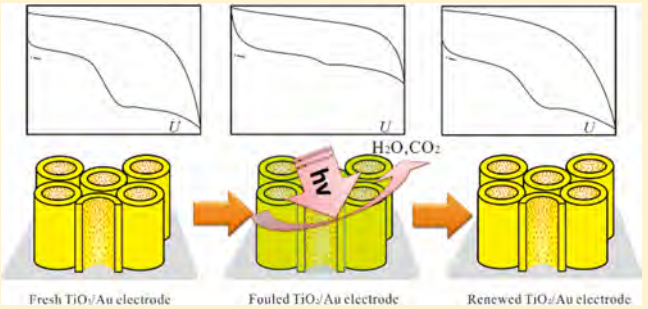

INTRODUCTION

Over the past decades, increasing scientific and public attention has been focused on endocrine disrupting chemicals (EDCs) because they are able to mimic or antagonize the effects of endogenous hormones, such as estrogens and androgens,[1,2] and influence the central nervous system as well as reproductive system in humans and wildlife.[3,4] Bisphenol A (2,2-bis(4-hydroxyphenol)propane, BPA) has been listed as a representative endocrine disrupter with widespread environmental contamination because it is an essential monomer for the production of high quality materials such as epoxy coating and polycarbonate plastic.[5−8] BPA has been found in numerous consumer products, including beverage packaging, baby bottles, reusable water bottles and food containers, flame retardants, adhesives, building materials, electronic components, and paper coatings.[5,7−11] It is widely present in aquatic environment, particularly in river water.[5,7−11] Toxicity studies have found that BPA may cause various adverse effects in the endocrine system of aquatic organisms even at low exposure levels.[5,12,13] Long-term BPA exposure has been associated with reproductive disorders including decline in sperm counts, increased birth defects, incidence of infertility, genital tract abnormalities, obesity, attention deficit hyperactivity, and prostate and breast cancer.[14−17] In September 2010, Canada became the first country to declare BPA a toxic substance and banned the use of BPA in baby bottles.[18] Therefore, it is very important to develop simple and rapid analytical methods to detect BPA at trace concentrations.

Various methods have been employed for the determination of BPA, including fluorescence,[19] liquid chromatography coupled with mass spectrometry,[20] high-performance liquid chromatography,[21] gas chromatography coupled with mass spectrometry,[22] enzyme linked immune sorbent assays (ELISA),[23] piezoelectric biosensing,[24] and electrochemical methods.[25−30] Electrochemistry is one of the preferred

Received: December 4, 2015
Revised: February 11, 2016
Accepted: March 22, 2016
Published: March 22, 2016

DOI: 10.1021/acs.est.5b05857
Environ. Sci. Technol. 2016, 50, 4430−4438

techniques in environmental and biological analysis because of its portability, simplicity, reliability, short analysis time, low power consumption, inexpensive equipment, and excellent sensitivity. Although a variety of electrochemical sensors have been proposed for BPA detection, the detection of BPA at traditional carbon or noble metal electrodes is compromised due to surface fouling and passivation by deposition of radical intermediates and electro-polymerized films of BPA,[29,31] leading to attenuated signal as well as reduced sensitivity and reproducibility over time.

Much effort has been expended to refresh the electrode surface in order to improve its reproducibility.[32] For example, polishable modified glassy carbon (GC)[33] and carbon paste[34] electrodes could be renewed by mechanical polishing, but this method cannot be applied to treat other nanostructured electrodes. Other methods such as vacuum annealing,[35] laser ablation,[36] flame etching,[37] chemical oxidative etching,[38] and electrochemical polarization[39] have also been used to refresh electrodes, but the harsh oxidization procedures easily lead to changes in surface chemistry and the microstructures, and thus affect electron-transfer kinetics and voltammetric background current.[32] Recently, we developed a strategy to refresh electrodes by UV or visible light irradiation without damaging the microstructure and chemical states of the electrodes, based on the property of photocatalytic degradation of organic compounds by carbon-doped TiO_2 nanotube arrays (TiO_2 NTAs).[40] In this study, we constructed a refreshable electrochemical sensor for detecting environmental pollutants such as BPA based on the TiO_2 NTAs. The intrinsic low electric conductivity and electrocatalytic activities of TiO_2 was overcome by modifying the TiO_2 NTAs with metal nanoparticles. Metal nanoparticles such as Au, Pt, and Ag nanoparticles are widely employed as modification materials to enhance the electrocatalytic activity and sensitivity due to their excellent conductivity and catalytic properties.[41,42] Meanwhile, metal nanoparticles are also widely used together with semiconductors to inhibit the recombination of photogenerated electrons and holes, therefore enhancing photocatalytic activities of the resulted heterostructures.[43−45] Herein, a highly sensitive and renewable electrode composed of gold nanoparticles (Au NPs) modified C-doped TiO_2 NTAs was fabricated by quick annealing of the as-anodized TiO_2 NTAs in argon followed by a facile, controllable electrodeposition of Au NPs. The electrode exhibits excellent electrochemical activity and high sensitivity for BPA because of the combination of electrocatalytic properties of Au NPs and photocatalytic activity of TiO_2/Au NTAs. To the best of our knowledge, this is the first time the electrocatalytic and photocatalytic properties of Au NPs were integrated with TiO_2 NTAs to detect BPA under UV irradiation. The results demonstrated that the Au−TiO_2 heterostructured NTAs exhibited higher sensitivity and larger linear range of BPA detection than either the TiO_2 NTAs with UV irradiation or the TiO_2/Au NTAs without UV irradiation.

MATERIALS AND METHODS

General. The standards of BPA, chloroauric acid ($HAuCl_4 \cdot H_2O$), NaH_2PO_4 and Na_2HPO_4, H_3PO_4, NaOH, NH_4F, Na_2SO_4, ethylene glycol were purchased from Sigma Chemical Co. The phosphate buffer solution (PBS, 0.1 M) was prepared by dissolving NaH_2PO_4 and Na_2HPO_4 in doubly distilled water (resistivity > 18 MΩ·cm), and the pH value was adjusted to 7.4 by adding H_3PO_4 and NaOH. All chemicals used were of analytical grade unless otherwise stated.

TiO_2/Au NTAs Fabrication and Characterization. The highly ordered C-doped TiO_2 NTAs electrode was fabricated by quick annealing of the as-anodized TiO_2 NTAs in argon in the absence of foreign carbonaceous precursors. The as-anodized TiO_2 NTAs were prepared by electrochemical anodization of a Ti metal foil in an NH_4F−ethylene glycol solution as described in our previous reports.[40,46] The distance between the graphite foil and Ti foil (2.0 × 1.0 × 0.1 cm^3, >99.6% purity, Goodfellow), which served as the cathode and anode respectively, is about 1 cm. The electrolyte was ethylene glycol containing 0.3 wt % NH_4F and 5 vol % doubly distilled water. Anodization was conducted at 60 V for 30 min using a direct current power supply (IT6834, ITECH, Nanjing, China). The anodized samples were rinsed by doubly distilled water, dried in air and then were annealed at 500 °C in a tube furnace under Ar at a heating rate of 15 °C·min^{-1}. The residual ethylene glycol resulting from the anodization process provided the carbon source for carbon-doping reaction. The electrodeposition was performed in a conventional three-electrode system by means of cyclic voltammetric scan from −1.25 V to −0.7 V (vs Ag/AgCl) for different cycles (1, 2, 5, 8, and 10 cycles, designed as TiO_2/Au-1, -2, -3, -4, and -5) at a scan rate of 50 mV·s^{-1} in a 0.1 M PBS (pH 7.4) containing 0.1 mM $HAuCl_4$. The morphology, structure, and composition of the samples were characterized by field-emission scanning electron microscopy (XL30 FE-SEM FEG, Philips Electron Optics, The Netherlands) equipped with energy dispersive X-ray (EDX), X-ray diffraction (XRD, Philips X' Pert Pro), X-ray photoelectron spectroscopy (XPS, ESCALB MK-II). In all XPS spectra, the binding energies were referenced to the Ar 2p peak at 242.4 eV.

Analytical Measurements and Calculations. Electrochemical measurements were performed in a conventional three-electrode system. The NTAs were insulated with epoxy resin exposing an area of 0.8 cm^2 as the working electrode. An Ag/AgCl electrode served as the reference electrode and a Pt foil was the counter electrode. All the electrochemical and photoelectrochemical experiments were carried out on a CHI614D potentiostat (CH Instruments Inc. Shanghai, China). The photoelectchemical property of the TiO_2 NTAs and TiO_2/Au NTAs were tested by amperometry (current−time) in a 0.5 M Na_2SO_4 solution. Electrode with surface fouling was generated by successive cyclic voltammetric scan for 10 cycles in 0.1 mM BPA in a 0.1 M PBS (pH 7.4). The contaminated electrode surface was regenerated by exposure to UV light for 30−180 min in doubly distilled water at room temperature. A monochromatic mercury lamp (375 nm) with photointensity of 5 mW·cm^{-2} was used as the UV light sources for UV treatment and photoelectrochemical experiments.

To study the utility of the TiO_2/Au NTAs electrode for BPA determination in environmental sample analysis, the interference test was performed in the presence of some common inorganic ions such as Na^+, K^+ Zn^{2+}, Ca^{2+}, Fe^{3+}, Cu^{2+}, SO_4^{2-}, NO_3^-, Cl^-, CO_3^-, and phenolic compounds such as phenol, 4-nitrophenol, 3,5-dimethylphenol, 4-fluorophenol. 0.5 μM and 1.0 μM BPA were spiked into a 50:50 PBS mixed tap water (pH 7.6) and seawater (pH 7.8) to estimate the recovery rate.

RESULTS AND DISCUSSION

Characterization of TiO_2 and TiO_2/Au NTAs. The anodized samples were annealed at 500 °C in a tube furnace under argon at a heating rate of 15 °C·min^{-1}. In the nanotube, owing to the nanoscale space confining effect,[47] the residual ethylene glycol resulting from the anodization process readily

DOI: 10.1021/acs.est.5b05857
Environ. Sci. Technol. 2016, 50, 4430−4438

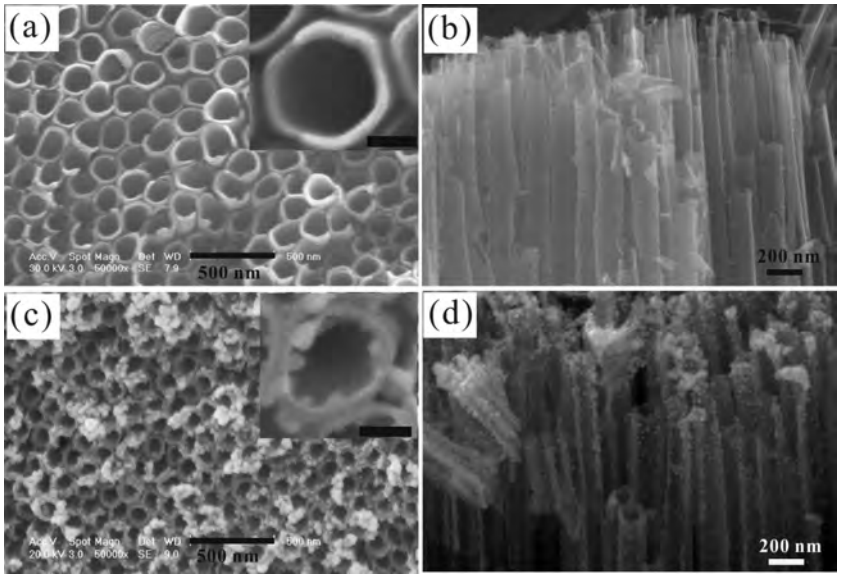

Figure 1. FE-SEM images of the top-surface (a, c) and cross section (b, d) morphology of TiO_2 NTAs (a, b) and TiO_2/Au NTAs (c, d), respectively. The insets in panels a and c are the enlarged top-view images of TiO_2 and TiO_2/Au nanotube, and the scale bar is 50 nm.

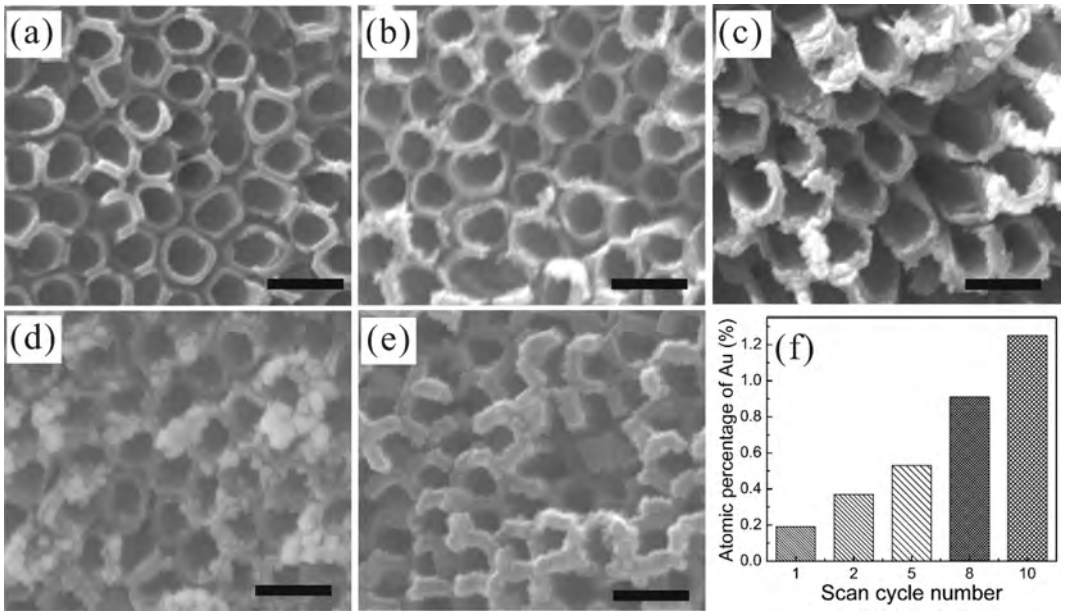

Figure 2. FE-SEM images of the top-view morphology of TiO_2/Au NTAs (a–e) with different amount of Au NPs loading. The scale bar is 200 nm. (f) Corresponding atomic percentage of Au detected by EDX.

reacted with TiO_2 to form C-doping TiO_2. Figure 1 shows the field-emission scanning electron microscopic (FE-SEM) images of the prepared C-doped TiO_2 NTAs (Figure 1a,b) and Au NPs modified C-doped TiO_2–NTAs (TiO_2/Au NTAs) (Figure 1c,d). The top- and cross-sectional views of the pristine smooth TiO_2 nanotubes (Figure 1a,b) showed an inner diameter of about 110 nm and a wall thickness of about 15 nm, with a length of approximately 7 μm (Supporting Information, SI, Figure S1). After Au NPs were coated onto the surface of TiO_2 NTAs by a facile electrodeposition with 8 cyclic voltammetric scan cycles in a 0.1 mM $HAuCl_4$ solution, the modified TiO_2 NTAs were covered with Au NPs of 10–15 nm diameter in the open ends of the nanotubes (Figure 1c). Underneath the top layer, smaller NPs with diameter of 4–8 nm were observed around the nanotube walls (both inside and outside) (Figure 1d). The distribution of Au NPs could be due to the capillary effect of the nanotubes which suppress the diffusion of $HAuCl_4$ solution into the NTAs.[43] Comparing the main diffractions peaks in X-ray diffraction (XRD) patterns (SI, Figure S2a), acquired from the TiO_2 NTAs and the modified TiO_2 NTAs, indicated that Au (JCPDS no. 04-0784) attached on the latter, which was further attested by X-ray photoelectron spectroscopy (XPS). The XPS survey scan spectrum (SI, Figure S2b) contained four kinds of elements, namely Ti (Ti 3s, 62.4 eV; Ti 2p3, 459.2 eV; Ti 2p1, 464.8 eV; Ti 2s, 566.4 eV), O (O 1s, 529.9 eV), C (C 1s, 284.6 eV), and Au (Au $4f_{7/2}$, 83.9 eV; Au $4f_{5/2}$, 87.4 eV; Au $4d_{5/2}$, 335.0 eV; Au $4d_{3/2}$, 352.9 eV),[48] respectively, suggesting the presence of gold on the surface of the modified NTAs.

DOI: 10.1021/acs.est.5b05857
Environ. Sci. Technol. 2016, 50, 4430–4438

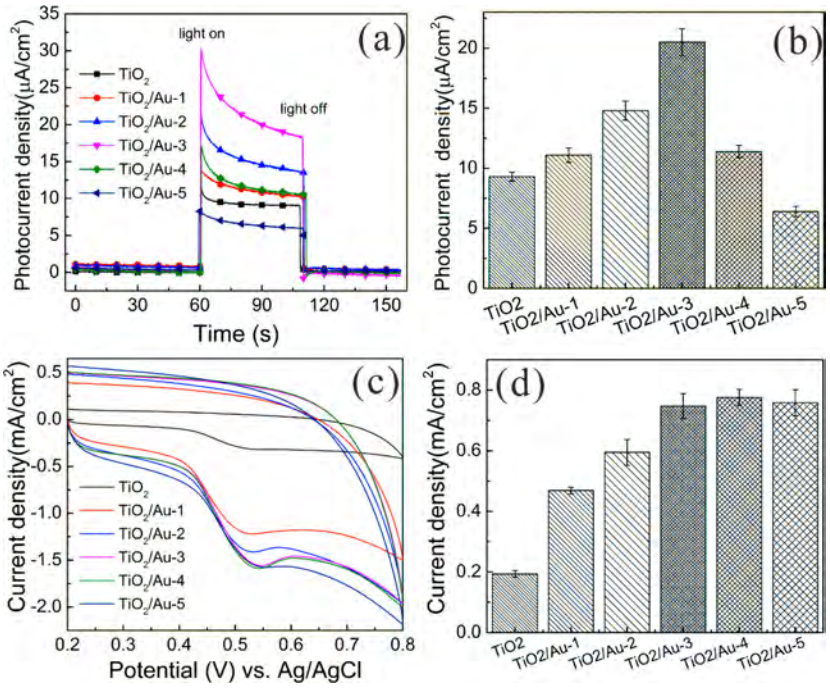

Figure 3. Photocurrent (i–t) plots (a) and steady current density (b) of different electrodes under UV light (375 nm) illumination at 0 V vs Ag/AgCl. Cyclic voltammetric profiles (c) and corresponding peak current density (d) of different electrodes in 0.1 M PBS (pH 7.4) containing 0.1 mM BPA at a scan rat of 100 mV·s^{-1}. The error bars represent the respond current of three independent experiments.

To optimize the electrocatalytic and photocatalytic properties, the nanotubes were modified with different amount of Au NPs by performing different cyclic voltammetric scan cycles. Figure 2a–c displays the FE-SEM images of TiO_2 NTAs coated with different amount of Au NPs, showing the thicknesses of the nanotube walls and the average sizes of the Au NPs increased gradually with the increased scan cycles. The accompanying energy dispersive X-ray (EDX) spectra (SI, Figure S3) suggested that the gold contents increased from ~0.19 to ~1.25 at. % from 1 to 10 voltammetric scan cycles (Figure 2f).

Photoelectrochemical and Electrochemical Performances. The TiO_2 NTAs and TiO_2/Au NTAs were insulated with epoxy resin exposing an area of 0.8 cm^2 as the working electrodes. The photoelectrochemical behaviors were first carried out by measuring the photocurrent response on TiO_2 NTAs and a series of TiO_2/Au NTAs electrodes with different amounts of Au NPs loading. Figure 3a presents the typical amperometric photocurrent density–time curves of TiO_2 NTAs and TiO_2/Au NTAs electrodes at 0 V bias vs Ag/AgCl with a pulse of 50 s under intermittent monochromatic mercury lamp (375 nm) irradiation. No photocurrent was produced in the dark for all electrodes, and the photocurrent was switched on under UV illumination. The photocurrent densities of all TiO_2/Au NTAs electrodes except TiO_2/Au-5 NTAs were higher than that of the bare carbon doped TiO_2 NTAs. The higher photocurrent density of TiO_2/Au NTAs electrodes signified an improved optical absorption capability because of Au NPs acting as conduction band (CB) electron traps to facilitate photogenerated electron (e^-)–hole (h^+) pair separation and effective transfer of the electrons to the electrode,[43−45] as compared to naked TiO_2 NTAs. For the TiO_2/Au NTAs electrodes, the photocurrent densities increased first and then decreased with increasing Au NPs loading. Among the steady photocurrent densities of the electrodes (Figure 3b), the highest value is about ~20.5 μA·cm^{-2} (obtained at TiO_2/Au-3 NTAs electrode), which is roughly 2 times that of the TiO_2 NTAs (~9.3 μA·cm^{-2}). Too much Au NPs decorated on the nanotubes (TiO_2/Au-4 and TiO_2/Au-5) caused photocurrents to decrease, probably due to the negative shading effect.[49,50] The shading effect implied that excessive Au NPs might lead to formation of much larger Au NPs covering the surface of TiO_2 NTAs, thus reducing the numbers of active sites available for absorbing light on TiO_2 NTAs.

The electrochemical performance of the TiO_2 NTAs and TiO_2/Au NTAs electrodes were studied by cyclic voltammetry using BPA as a redox probe. Figure 3c shows the cyclic voltammograms acquired from the TiO_2 NTAs and TiO_2/Au-1, -2, -3, -4, and -5 NTAs electrodes in 0.1 M PBS (pH 7.4) containing 0.1 mM BPA at a scanning rate of 100 mV·s^{-1} from 0.2 to 0.8 V. A well-defined oxidation peak was observed at both TiO_2 NTAs and TiO_2/Au NTAs electrodes, whereas no corresponding reduction peaks was observed. This is attributed to irreversible oxidation of the hydroxyl group present in the aromatic ring of the BPA to form phenonium ions, a kind of phenoxy radical.[29,51,52] Compared to the bare TiO_2 NTAs electrode, the oxidation currents of BPA at TiO_2/Au NTAs electrodes increased significantly. This electrocatalytic activity toward BPA could be due to the unique electronic properties of the Au NPs which may accelerate the electron transfer rate via improved conductivity and high specific surface area. The peak current increased sharply from ~0.47 mA·cm^{-2} at TiO_2/Au-1 to ~0.60 mA·cm^{-2} at TiO_2/Au-2, and to ~0.75 mA·cm^{-2} at TiO_2/Au-3, and reached saturation level at TiO_2/Au-4 (~0.77 mA·cm^{-2}), and eventually dropped to ~0.75 mA·cm^{-2} at TiO_2/Au-5 (Figure 3d). The peak density drop may result from decrease of the reaction surface area due to excessive NPs coated on the NTAs walls (Figure 2e). The electrochemical performance of the TiO_2/Au NTAs electrodes toward BPA

DOI: 10.1021/acs.est.5b05857
Environ. Sci. Technol. 2016, 50, 4430−4438

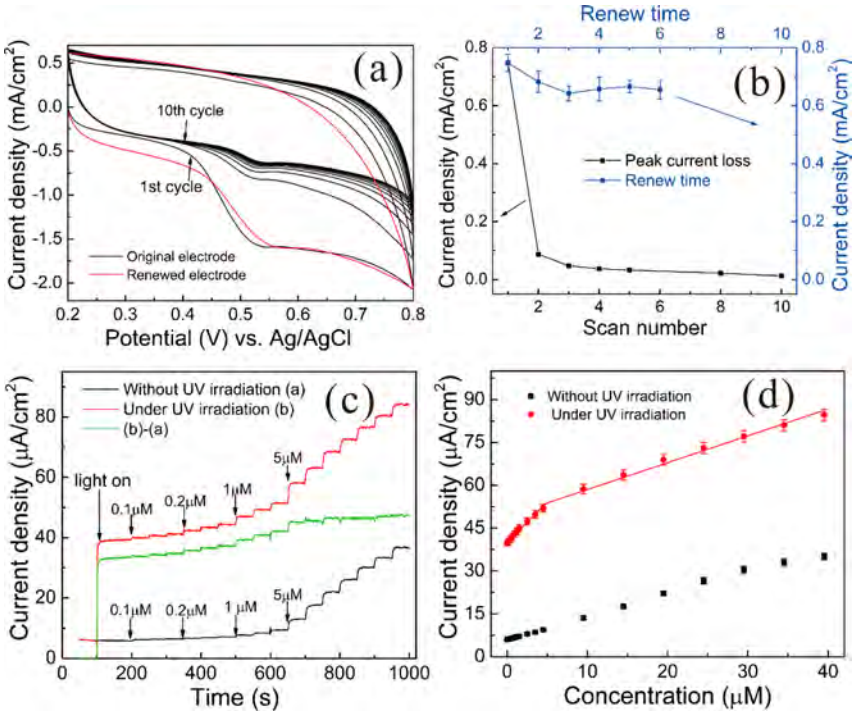

Figure 4. (a) Cyclic voltammograms of 0.1 mM BPA in 0.1 M (pH 7.4) PBS obtained from original (black) and renewed (red) TiO_2/Au-3 NTAs electrode. Scan rate: 100 mV·s^{-1}. (b) Peak current of different scan number (black) and renew times (blue). (c) Current−time recording obtained at TiO_2/Au-3 NTAs electrode with successive addition of 0.1 μM−5.0 μM BPA into a stirred 0.1 M PBS (pH 7.4) at an applied potential of 530 mV with (red)/without (black) UV irradiation, with the result (green) of subtracting of black line from red line. (d) Calibration curve of the respond currents versus concentrations of BPA with/without UV irradiation. The error bars represent the respond current of three independent experiments.

suggested that the amount of Au NPs loaded on TiO_2 NTAs could be readily optimized.

Analytical Response. On the basis of the above evaluation, we combined the photoelectrochemical and electrochemical properties of TiO_2/Au-3 NTAs to develop a sensitive and refreshable electrochemical sensor for BPA detection. During BPA electrochemical detection, electrodes usually suffered from severe drop in amperometric or voltammetric signal over time due to oxidative and polymeric products of BPA depositing on the electrode surface, resulting in the passivation of the electrodes.[29,31] Surface fouling presents a major challenge in the reproducibility and stability, and thus the sensitivity and selectivity of BPA detection. It is well-known that accumulated oxidative or polymeric products of BPA on semiconductor surfaces (e.g., TiO_2) can be photocatalytically degraded under UV or visible irradiation.[53,54] As shown above, TiO_2/Au NTAs has shown excellent photoelectrochemical property. Thus, the TiO_2/Au electrode could be photocatalytically refreshed to maintain good reproducibility and stability.

Figure 4a shows the cyclic voltammetric profiles of 0.1 mM BPA in PBS on the original TiO_2/Au-3 NTAs by scanning between 0.2 and 0.8 V with a rate of 100 mV·s^{-1}. A well-defined strong oxidation peak corresponding to BPA was observed at about ~530 mV in the first cycle, whereas the peak current decreased gradually in subsequent cycles due to irreversible electrochemical oxidation of BPA.[51,52] The oxidative and polymeric products of BPA deposited on the electrode surface insulated and blocked further oxidation of BPA monomer completely.[29,31] The contaminated electrode surface was renewed by exposure to UV light for 30−180 min. The results showed that the peak currents assigned to BPA responses increased with increasing irradiation time (SI, Figure S4), and the cyclic voltammetric curve returned almost fully to its original shape and magnitude after 120 min of illumination (Figure 4a, red line; Figure S4). The sensitivity of the electrode after five fouling/refreshing runs was still similar to that in the first cycle, with a relative standard deviation (RSD) of 3.0% (n = 5, Figure 4b), showing excellent reproducibility.

Figure 4c displays a typical current−time plots of TiO_2/Au-3 NTAs with successive injection of BPA of concentrations ranging from 0.1 μM to 5.0 μM into the stirred PBS (0.1 M, pH 7.4) at 530 mV with (red line) or without (black line) UV illumination, respectively. The current was near zero in the dark and then jumped sharply after switching on the light (Figure 4c, red line). When BPA was added into the stirred solution, the current further increased immediately (Figure 4c, red line). Obviously, the amperometric response of BPA is much larger than that without UV illumination. The greater BPA signal could be attributed to both electrochemical oxidation of BPA and increased photocurrent (Figure 4c, green line (result of subtracting black line from red line)) due to the improved separation efficiency of the photogenerated electron (e-)−hole (h+) pairs derived from the consumption of holes by BPA.[55] No apparent further enhancements were observed when the concentration of injected BPA increased to 5 μM (Figure 4c, green line), where the enhancement of photocurrent reached the maximum and the electrode was fouled because of the high concentration of BPA. Figure 4d presents the calibration plots of TiO_2/Au-3 NTAs without (black) and with UV light irradiation (red), respectively. Without irradiation, the analytical signals exhibited a linear range from 0.1 to 28.9 μM, with a correlation coefficient of 0.9955 and sensitivity of 0.81 μA·μM^{-1}·cm^{-2}. The limit of detection (LOD) was calculated to be 4.7 × 10^{-8} M (S/N = 3), which is comparable

DOI: 10.1021/acs.est.5b05857
Environ. Sci. Technol. 2016, 50, 4430−4438

Table 1. Comparison of the Proposed Method to Other Sensors Based on Different Electrodes for BPA Detection[a]

electrode	sensitivity (μA μM^{-1} cm^{-2})	linear range (M)	detection limit (M)	reference
Pt/graphene−CNTs/GCE		1.0×10^{-8} to 8×10^{-5}	4.2×10^{-8}	29
AuNPs/SGNF/GCE	0.91	8.0×10^{-8} to 2.5×10^{-4}	3.5×10^{-8}	57
PGA/MWCNT-NH_2/GCE	0.82	1.0×10^{-7} to 1.0×10^{-5}	2.0×10^{-8}	58
MNPs/rGO/GCE	0.25	6.0×10^{-8} to 1.1×10^{-5}	1.7×10^{-8}	59
MWCNT- melamine/GCE	1.01	1.0×10^{-8} to 4.1×10^{-5}	5.0×10^{-9}	30
GR/Au-Tyr-CS/GCE	0.51	2.5×10^{-8} to 3×10^{-6}	1.0×10^{-9}	60
Tyr−rGO−DAPPT/GCE		1.0×10^{-9} to 3.8×10^{-5}	3.5×10^{-10}	26*
Tyr-diazonium-MWCNTs/BDD	1.81	1.0×10^{-11} to 1.0×10^{-7}	1.0×10^{-11}	27*
TiO_2/Au NTAs	0.81	1.0×10^{-7} to 2.89×10^{-5}	4.7×10^{-8}	our work (without UV irradiation)
	2.8	1.0×10^{-7} to 3.89×10^{-5}	6.2×10^{-9}	our work (with UV irradiation)

[a]CNT, carbon nanotubes; GCE, glass carbon electrode; SWNT, single walled CNT; SGNF, stacked graphene nanofibers; AuNPs, gold nanoparticles; rGO, reduced graphene oxide; MNPs, magnetic nanoparticles; PGA, polyglutamate acid; Tyr, tyrosinase; DAPPT, 1,3-di(4-amino-1-pyridinium)propane tetrafluoroborate; BDD, boron-doped diamond; *, enzyme enhanced.

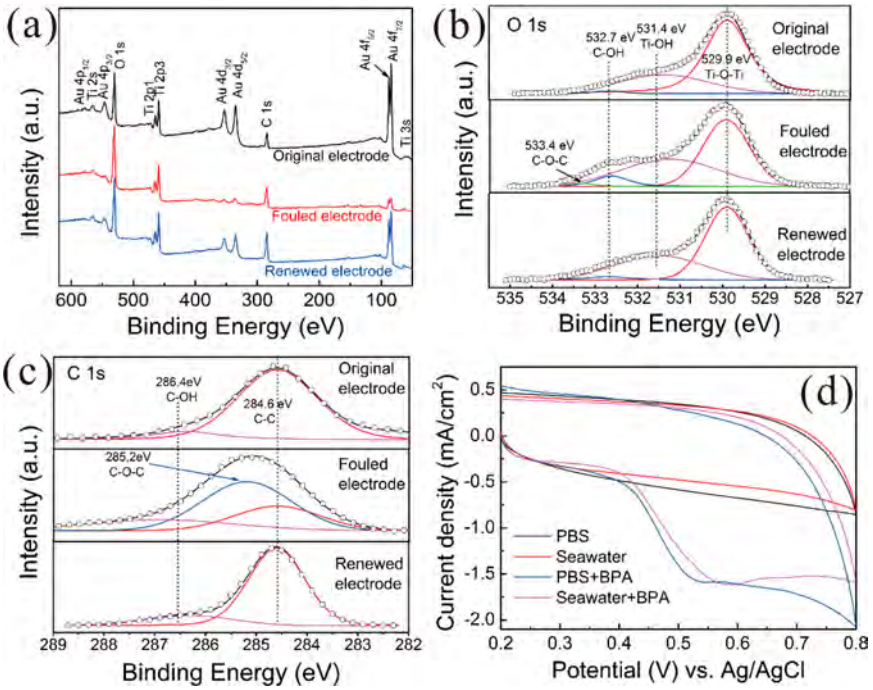

Figure 5. XPS surface scan spectrum (a), high-resolution O 1s (b) and C 1s (b) XPS spectra of fresh, fouled and renewed TiO_2/Au-3 NTAs electrode. (d) Cyclic voltammograms of 0 and 0.1 mM BPA in 0.1 M PBS (pH 7.4) and seawater obtained at TiO_2/Au-3 NTAs electrode, respectively. Scanning rate: 100 mV·s^{-1}.

to most of the reported values in the literatures (Table 1).[26−30,57−60] With UV illumination, the calibration curve consists of two linear sections, one ranging from 0.1 to 4.9 μM with a correlation coefficient of 0.9901 and sensitivity of 2.8 μA·μM^{-1}·cm^{-2}, and another from 4.9 to 38.9 μM with a correlation coefficient of 0.9892 and sensitivity of 0.94 μA·μM^{-1}·cm^{-2}. The LOD was calculated as 6.2×10^{-9} M (S/N = 3), which is lower than those nonenzymatic electrochemical sensors reported previously (Table 1).[26−30,57−60] The increased sensitivity and decreased LOD with UV irradiation was due to further enhanced photocurrent after adding BPA. The widened linear range was attributed to the photocleaning effect of TiO_2/Au NTAs electrode which provide a fresh surface with high electrocatalytic activities continuously. As a control, BPA detection on TiO_2 NTAs electrode with UV irradiation was also carried out, where the sensitivity was lower (1.36 μA·μM^{-1}·cm^{-2}) and LOD was greater (2×10^{-8} M) than the TiO2/Au NTAs (SI, Figure S5). It is clear that the enhanced electrochemical performance of the TiO_2/Au NTAs electrode was due to the improved photocatalytic property of Au NPs.

XPS was used to determine the surface chemical composition (Figure 5a−c) in order to evaluate the changing surface states of the original, fouled and photocatalytically renewed TiO_2/Au NTAs electrodes. The results (Figure 5a) showed that the electrodes consisted of the same elements (Ti, O, C, and Au) in different states, whereas the peak intensities of Au obtained from the fouled electrode were much lower than that of the original and refreshed electrodes. The high-resolution O 1s spectra (Figure 5b) of the electrodes showed that, in addition to the three peaks located at 529.9, 531.4, and 532.7 eV, which correspond to Ti−O−Ti, Ti−OH, and C−OH bonds, respectively, there was a small peak corresponding to C−O−C (533.4 eV) bond[56] in the fouled electrode. The intensity corresponds to C−OH (532.7 eV) bond also increased markedly in the fouled electrodes compared to the original or

DOI: 10.1021/acs.est.5b05857
Environ. Sci. Technol. 2016, 50, 4430−4438

the renewed electrodes. This was corroborated by the high-resolution C 1s spectra (Figure 5c). The C−O−C bond signal was derived from the absorbed and/or electrochemical oxidized or polymerized products of BPA. However, after UV light irradiation for 2 h, the chemical states of the electrode recovered to the original conditions, and the peaks in O 1s and C 1s spectra associated with C−O−C bonds disappeared. Under UV light illumination, the absorbed intermediate species could be easily decomposed[53,54] without damaging the surface microstructure of the electrode.

Interference and Practical Application. To evaluate the selectivity of the electrochemical sensor, BPA (1.0 μM) detection was carried out in the presence of some common phenolic derivatives and inorganic ions to detect any interference. The results showed that 100-fold of Na^+, K^+ Zn^{2+}, Ca^{2+}, Fe^{3+}, Cu^{2+}, SO_4^{2-}, NO_3^-, Cl^-, CO_3^-, and 20-fold of phenolic derivatives such as phenol, 4-nitrophenol, 3,5-dimethylphenol, and 4-fluorophenol have no obvious effect on the response to BPA with deviations below 5% (SI, Figure S6), indicating the sensor has good selectivity for BPA detection.

To validate further the field application potential of the BPA sensor, we conducted cyclic voltammtric BPA detection in 0.22 μm membrane filtered seawater (pH 7.8) first, and then determined the BPA content in a 50:50 PBS mixed tap water (pH 7.6) and seawater, with 0.5 and 1.0 μM BPA, respectively. Compared to the results obtained in PBS, similar cyclic voltammtric performance for BPA detection was observed except a slight shift in the potential value due to the pH effect (Figure 5d), suggesting the feasibility of using the electrochemical sensor in fresh and seawater. Table 2 tabulates the

Table 2. Recovery of Spiked BPA in Natural Water (n = 3)

sample	measured (μM)	spiked (μM)	found (μM)	recovery (%)	RSD (%)
tap water	0	0.5	0.52	104	3.6
		1.0	0.95	95	4.7
seawater	0	0.5	0.51	102	5.2
		1.0	1.07	107	4.1

performance of the analytical method on various sample matrices. The results showed that no BPA was detected in both tap water and seawater, and the recoveries of BPA ranged from 95% to 104% for spiked tap water, and 102% to 107% for spiked seawater, respectively, and the RSD (n = 3) was less than 5.2% for 3 successive assays. This result is comparable to other methods, where the recoveries of BPA were reported in the range between 94% and 109.2%.[26−30,57−60]

In summary, a photoassisted refreshable electrode based on Au nanoparticle modified C-doped TiO_2 nanotube arrays (NTAs) was developed for sensitive and reproducible BPA detection. The Au nanoparticles decorated on the tubular walls of self-organized TiO_2 NTAs improved both the photoelectrocatalytic activity and the electrocatalytic properties of the electrode. A key advantage of the high photocatalytic activity of TiO_2/Au NTAs is that UV irradiation can be used during the detection processes to refresh the electrode surface with high electrocatalytic activities continuously and enhance the amperometric response of BPA. The electrochemical sensor showed a large linear range, increased sensitivity, and decreased LOD for BPA detection with the ability to remove surface fouling. The results demonstrated that the TiO_2/Au NTAs electrode has great potential as a sensitive and recyclable electrochemical sensing platform for online monitoring of BPA and other electrochemically active environmental pollutants or pharmaceutical residues.

■ ASSOCIATED CONTENT

Supporting Information

The Supporting Information is available free of charge on the ACS Publications website at DOI: 10.1021/acs.est.5b05857.

FE-SEM of the side-view image morphology of of TiO_2 NTAs, XRD patterns and XPS surface scan spectrum, EDX spectra, cyclic voltammograms, current−time recording obtained at TiO_2 electrode and calibration curve of the respond currents versus concentrations of BPA with/without UV irradiation, and current−time recording obtained at TiO_2/Au-3 NTAs electrode (PDF).

■ AUTHOR INFORMATION

Corresponding Author

*Mengsu Yang. Tel: (852) 34427797. Fax: (852) 34420552. E-mail: bhmyang@cityu.edu.hk.

Author Contributions

L.H. designed and performed the electrochemical experiments, and wrote the paper. C.-C.F. designed the experiments, discussed and analyzed the data. X.Z. characterized the electrodes and carried out the photoelectrocatalytic experiments. L.L.C. and P.K.S.L. provided technical support. P.K.C. and K.-Y.W. discussed the data and edited the paper. M.Y. initiated, designed, and supervised the project and edited the paper. All authors have given approval to the final version of the paper.

Notes

The authors declare no competing financial interest.

■ ACKNOWLEDGMENTS

This study was supported by grants from the General Research Fund (CityU-103312), State Key Laboratory in Marine Pollution, City University of Hong Kong, and Basic Research Fund from Shenzhen Municipal Government.

■ REFERENCES

(1) Krishnan, A. V.; Stathis, P.; Permuth, S. F.; Tokes, L.; Feldman, D. Bisphenol A: an estrogenic substance is released from polycarbonate flasks during autoclaving. *Endocrinology* **1993**, *132* (6), 2279−2286.

(2) Tabb, M. M.; Blumberg, B. New modes of action for endocrine-disrupting chemicals. *Mol. Endocrinol.* **2006**, *20* (3), 475−482.

(3) Colborn, T.; vom Saal, F. S.; Soto, A. M. Developmental effects of endocrine-disrupting chemicals in wildlife and humans. *Environ. health persp.* **1993**, *101* (5), 378−384.

(4) Waring, R.; Harris, R. Endocrine disrupters: a human risk? *Mol. Cell. Endocrinol.* **2005**, *244* (1), 2−9.

(5) Staples, C. A.; Dome, P. B.; Klecka, G. M.; Oblock, S. T.; Harris, L. R. A review of the environmental fate, effects, and exposures of bisphenol A. *Chemosphere* **1998**, *36* (10), 2149−2173.

(6) Ash, I.; Ash, M. *Handbook of plastic and rubber additives*; Synapse Information Resources: Endicott, NY, 2005.

(7) Vandenberg, L. N.; Chahoud, I.; Heindel, J. J.; Padmanabhan, V.; Paumgartten, F. J.; Schoenfelder, G. Urinary, circulating, and tissue biomonitoring studies indicate widespread exposure to bisphenol A. *Cien. saude colet.* **2012**, *17* (2), 407−434.

DOI: 10.1021/acs.est.5b05857
Environ. Sci. Technol. 2016, 50, 4430−4438

(8) Vandenberg, L. N.; Chahoud, I.; Heindel, J. J.; Padmanabhan, V.; Paumgartten, F. J.; Schoenfelder, G. Urinary, circulating, and tissue biomonitoring studies indicate widespread exposure to bisphenol A. *Environ. health persp.* **2010**, *118* (8), 1055−1070.
(9) Kolpin, D. W.; Furlong, E. T.; Meyer, M. T.; Thurman, E. M.; Zaugg, S. D.; Barber, L. B.; Buxton, H. T. Pharmaceuticals, hormones, and other organic wastewater contaminants in US streams, 1999−2000: A national reconnaissance. *Environ. Sci. Technol.* **2002**, *36* (6), 1202−1211.
(10) Vandenberg, L. N.; Hauser, R.; Marcus, M.; Olea, N.; Welshons, W. V. Human exposure to bisphenol A (BPA). *Reprod. Toxicol.* **2007**, *24* (2), 139−177.
(11) Schecter, A.; Malik, N.; Haffner, D.; Smith, S.; Harris, T. R.; Paepke, O.; Birnbaum, L. Bisphenol A (BPA) in US Food. *Environ. Sci. Technol.* **2010**, *44* (24), 9425−9430.
(12) Barata, C.; Porte, C.; Baird, D. J. Experimental designs to assess endocrine disrupting effects in invertebrates a review. *Ecotoxicology* **2004**, *13* (6), 511−517.
(13) Brennan, S. J.; Brougham, C. A.; Roche, J. J.; Fogarty, A. M. Multi-generational effects of four selected environmental oestrogens on Daphnia magna. *Chemosphere* **2006**, *64* (1), 49−55.
(14) Delbès, G.; Levacher, C.; Habert, R. Estrogen effects on fetal and neonatal testicular development. *Reproduction* **2006**, *132* (4), 527−538.
(15) Hamid, H.; Eskicioglu, C. Fate of estrogenic hormones in wastewater and sludge treatment: A review of properties and analytical detection techniques in sludge matrix. *Water Res.* **2012**, *46* (18), 5813−5833.
(16) Thompson, C.; Berl, T.; Tejedor, A.; Johannsson, G. Differential diagnosis of hyponatraemia. *Best Pract. Res. Clin. Endocrinol. Metab.* **2012**, *26* (1), S7−S15.
(17) Gerona, R. R.; Woodruff, T. J.; Dickenson, C. A.; Pan, J.; Schwartz, J. M.; Sen, S.; Friesen, M. W.; Fujimoto, V. Y.; Hunt, P. A. Bisphenol-A (BPA), BPA glucuronide, and BPA sulfate in midgestation umbilical cord serum in a northern and central California population. *Environ. Sci. Technol.* **2013**, *47* (21), 12477−12485.
(18) Egan, L. Canada declares BPA toxic, sets stage for more bans. http://fryngе.com/work/babyfriendly/may06/Canada%20declares%20BPA%20toxic%20101410.pdf.
(19) Yoon, Y.; Westerhoff, P.; Snyder, S. A.; Esparza, M. HPLC-fluorescence detection and adsorption of bisphenol A, 17β-estradiol, and 17α-ethynyl estradiol on powdered activated carbon. *Water Res.* **2003**, *37* (14), 3530−3537.
(20) Sambe, H.; Hoshina, K.; Hosoya, K.; Haginaka, J. Direct injection analysis of bisphenol A in serum by combination of isotope imprinting with liquid chromatography-mass spectrometry. *Analyst* **2005**, *130* (1), 38−40.
(21) Sajiki, J.; Takahashi, K.; Yonekubo, J. Sensitive method for the determination of bisphenol-A in serum using two systems of high-performance liquid chromatography. *J. Chromatogr., Biomed. Appl.* **1999**, *736* (1), 255−261.
(22) Zhang, J.; Cooke, G. M.; Curran, I. H.; Goodyer, C. G.; Cao, X. L. GC−MS analysis of bisphenol A in human placental and fetal liver samples. *J. Chromatogr. B: Anal. Technol. Biomed. Life Sci.* **2011**, *879* (2), 209−214.
(23) Zhao, M.-P.; Li, Y.-Z.; Guo, Z.-Q.; Zhang, X.-X.; Chang, W.-B. A new competitive enzyme-linked immunosorbent assay (ELISA) for determination of estrogenic bisphenols. *Talanta* **2002**, *57* (6), 1205−1210.
(24) Hu, L. S.; Fong, C. C.; Zou, L.; Wong, W. L.; Wong, K. Y.; Wu, R. S.; Yang, M. Label-free detection of endocrine disrupting chemicals by integrating a competitive binding assay with a piezoelectric ceramic resonator. *Biosens. Bioelectron.* **2014**, *53*, 406−413.
(25) Qu, Y.; Ma, M.; Wang, Z.; Zhan, G.; Li, B.; Wang, X.; Fang, H.; Zhang, H.; Li, C. Sensitive amperometric biosensor for phenolic compounds based on graphene−silk peptide/tyrosinase composite nanointerface. *Biosens. Bioelectron.* **2013**, *44*, 85−88.
(26) Li, R.; Wang, Y.; Deng, Y.; Liu, G.; Hou, X.; Huang, Y.; Li, C. Enhanced Biosensing of Bisphenol A Using a Nanointerface Based on Tyrosinase/Reduced Graphene Oxides Functionalized with Ionic Liquid. *Electroanalysis* **2016**, *28* (1), 96−102.
(27) Zehani, N.; Fortgang, P.; Lachgar, M. S.; Baraket, A.; Arab, M.; Dzyadevych, S. V.; Kherrat, R.; Jaffrezic-Renault, N. Highly sensitive electrochemical biosensor for bisphenol A detection based on a diazonium-functionalized boron-doped diamond electrode modified with a multi-walled carbon nanotube-tyrosinase hybrid film. *Biosens. Bioelectron.* **2015**, *74*, 830−835.
(28) Kim, K. S.; Jang, J. R.; Choe, W. R.; Yoo, P. J. Electrochemical detection of Bisphenol A with high sensitivity and selectivity using recombinant protein-immobilized graphene electrodes. *Biosens. Bioelectron.* **2015**, *71*, 214−221.
(29) Zheng, Z.; Du, Y.; Wang, Z.; Feng, Q.; Wang, C. Pt/graphene−CNTs nanocomposite based electrochemical sensors for the determination of endocrine disruptor bisphenol A in thermal printing papers. *Analyst* **2013**, *138* (2), 693−701.
(30) Li, Y.; Gao, Y.; Cao, Y.; Li, H. Electrochemical sensor for bisphenol A determination based on MWCNT/melamine complex modified GCE. *Sens. Actuators, B* **2012**, *171*, 726−733.
(31) Murugananthan, M.; Yoshihara, S.; Rakuma, T.; Shirakashi, T. Mineralization of bisphenol A (BPA) by anodic oxidation with boron-doped diamond (BDD) electrode. *J. Hazard. Mater.* **2008**, *154* (1), 213−220.
(32) Zoski, C. G. *Handbook of Electrochemistry*; Elsevier: Amsterdam, 2007.
(33) Aihara, M.; Komatsu, M. Activation of glassy carbon electrodes by polishing with ceramics particles. *Bull. Chem. Soc. Jpn.* **1987**, *60* (5), 1911−1912.
(34) Wang, J.; Varughese, K. Polishable and robust biological electrode surfaces. *Anal. Chem.* **1990**, *62* (3), 318−320.
(35) Fagan, D. T.; Hu, I. F.; Kuwana, T. Vacuum heat-treatment for activation of glassy carbon electrodes. *Anal. Chem.* **1985**, *57* (14), 2759−2763.
(36) Brennan, J. L.; Forster, R. J. Laser light and electrodes: Interaction mechanisms and electroanalytical applications. *J. Phys. Chem. B* **2003**, *107* (35), 9344−9350.
(37) Strand, A. M.; Venton, B. J. Flame etching enhances the sensitivity of carbon-fiber microelectrodes. *Anal. Chem.* **2008**, *80* (10), 3708−3715.
(38) Johnson, D. C.; LaCourse, W. R. Liquid chromatography with pulsed electrochemical detection at gold and platinum electrodes. *Anal. Chem.* **1990**, *62* (10), 589A−597A.
(39) Takmakov, P.; Zachek, M. K.; Keithley, R. B.; Walsh, P. L.; Donley, C.; McCarty, G. S.; Wightman, R. M. Carbon microelectrodes with a renewable surface. *Anal. Chem.* **2010**, *82* (5), 2020−2028.
(40) Hu, L. S.; Huo, K. F.; Chen, R. S.; Gao, B.; Fu, J.; Chu, P. K. Recyclable and high-sensitivity electrochemical biosensing platform composed of carbon-doped TiO_2 nanotube arrays. *Anal. Chem.* **2011**, *83* (21), 8138−8144.
(41) Xiao, F. Layer-by-layer self-assembly construction of highly ordered metal-TiO_2 nanotube arrays heterostructures (M/TNTs, M= Au, Ag, Pt) with tunable catalytic activities. *J. Phys. Chem. C* **2012**, *116* (31), 16487−16498.
(42) Gao, Z. D.; Han, Y. Y.; Li, Y. C.; Yang, M.; Song, Y. Y. Photocatalytic synthesis and synergistic effect of Prussian blue-decorated Au nanoparticles/TiO_2 nanotube arrays for H_2O_2 amperometric sensing. *Electrochim. Acta* **2014**, *125*, 530−535.
(43) Xu, Z.; Lin, Y.; Yin, M.; Zhang, H.; Cheng, C.; Lu, L.; Xue, X.; Fan, H. J.; Chen, X.; Li, D. Understanding the Enhancement Mechanisms of Surface Plasmon-Mediated Photoelectrochemical Electrodes: A Case Study on Au Nanoparticle Decorated TiO_2 Nanotubes. *Adv. Mater. Interfaces* **2015**, *2*, DOI: 10.1002/admi.201500169.
(44) Xiao, F. X.; Hung, S. F.; Miao, J.; Wang, H. Y.; Yang, H.; Liu, B. Metal-Cluster-Decorated TiO_2 Nanotube Arrays: A Composite Heterostructure toward Versatile Photocatalytic and Photoelectrochemical Applications. *Small* **2015**, *11* (5), 554−567.
(45) Chen, Z. F.; Huang, X. F.; Liu, M. C.; Zhao, G. H. High-Yield and Selective Photoelectrocatalytic Reduction of CO_2 to Formate by

DOI: 10.1021/acs.est.5b05857
Environ. Sci. Technol. 2016, 50, 4430−4438

Metallic Copper Decorated Co_3O_4 Nanotube Arrays. *Environ. Sci. Technol.* **2015**, *49* (9), 5828−5835.
(46) Huo, K. F.; Li, Y.; Chen, R. S.; Gao, B.; Peng, C.; Zhang, W. J.; Hu, L. S.; Zhang, X. M.; Chu, P. K. Recyclable Non-Enzymatic Glucose Sensor Based on $Ni/NiTiO_3/TiO_2$ Nanotube Arrays. *ChemPlusChem* **2015**, *80* (3), 576−582.
(47) Pan, X. L.; Fan, Z. L.; Chen, W.; Ding, Y. J.; Luo, H. Y.; Bao, X. H. Enhanced ethanol production inside carbon-nanotube reactors containing catalytic particles. *Nat. Mater.* **2007**, *6* (7), 507−511.
(48) Moulder, J. F.; Chastain, J.; King, R. C. *Handbook of X-ray photoelectron spectroscopy: a reference book of standard spectra for identification and interpretation of XPS data*; Perkin-Elmer: Eden Prairie, MN, 1992.
(49) Hou, Y.; Laursen, A. B.; Zhang, J.; Zhang, G.; Zhu, Y.; Wang, X.; Dahl, S.; Chorkendorff, I. Layered Nanojunctions for Hydrogen-Evolution Catalysis. *Angew. Chem., Int. Ed.* **2013**, *52* (13), 3621−3625.
(50) Wang, M.; Sun, L.; Lin, Z.; Cai, J.; Xie, K.; Lin, C. p−n Heterojunction photoelectrodes composed of Cu_2O-loaded TiO_2 nanotube arrays with enhanced photoelectrochemical and photoelectrocatalytic activities. *Energy Environ. Sci.* **2013**, *6* (4), 1211−1220.
(51) Kuramitz, H.; Nakata, Y.; Kawasaki, M.; Tanaka, S. Electrochemical oxidation of bisphenol A. Application to the removal of bisphenol A using a carbon fiber electrode. *Chemosphere* **2001**, *45* (1), 37−43.
(52) Kuramitz, H.; Matsushita, M.; Tanaka, S. Electrochemical removal of bisphenol A based on the anodic polymerization using a column type carbon fiber electrode. *Water Res.* **2004**, *38* (9), 2331−2338.
(53) Guo, C.; Ge, M.; Liu, L.; Gao, G.; Feng, Y.; Wang, Y. Directed synthesis of mesoporous TiO_2 microspheres: catalysts and their photocatalysis for bisphenol A degradation. *Environ. Sci. Technol.* **2010**, *44* (1), 419−425.
(54) Wang, C.; Zhang, H.; Li, F.; Zhu, L. Degradation and mineralization of bisphenol A by mesoporous Bi_2WO_6 under simulated solar light irradiation. *Environ. Sci. Technol.* **2010**, *44* (17), 6843−6848.
(55) Pardo-Yissar, V.; Katz, E.; Wasserman, J.; Willner, I. Acetylcholine esterase-labeled CdS nanoparticles on electrodes: photoelectrochemical sensing of the enzyme inhibitors. *J. Am. Chem. Soc.* **2003**, *125* (3), 622−623.
(56) Beamson, G.; Briggs, D. The scienta ESCA 300 database. In *High Resolution XPS of Organic Polymers*; John Wiley & Sons: New York, 1992.
(57) Niu, X.; Yang, W.; Wang, G.; Ren, J.; Guo, H.; Gao, J. A novel electrochemical sensor of bisphenol A based on stacked graphene nanofibers/gold nanoparticles composite modified glassy carbon electrode. *Electrochim. Acta* **2013**, *98*, 167−175.
(58) Lin, Y.; Liu, K.; Liu, C.; Yin, L.; Kang, Q.; Li, L.; Li, B. Electrochemical sensing of bisphenol A based on polyglutamic acid/amino-functionalised carbon nanotubes nanocomposite. *Electrochim. Acta* **2014**, *133*, 492−500.
(59) Zhang, Y.; Cheng, Y.; Zhou, Y.; Li, B.; Gu, W.; Shi, X.; Xian, Y. Electrochemical sensor for bisphenol A based on magnetic nanoparticles decorated reduced graphene oxide. *Talanta* **2013**, *107*, 211−218.
(60) Pan, D.; Gu, Y.; Lan, H.; Sun, Y.; Gao, H. Functional graphene-gold nano-composite fabricated electrochemical biosensor for direct and rapid detection of bisphenol A. *Anal. Chim. Acta* **2015**, *853*, 297−302.

DOI: 10.1021/acs.est.5b05857
Environ. Sci. Technol. 2016, 50, 4430−4438

Supporting Information

Au Nanoparticles Decorated TiO_2 Nanotube Arrays as a Recyclable Sensor for Photoenhanced Electrochemical Detection of Bisphenol A

Liangsheng Hu[†,∥], Chi-Chun Fong[†,‡,⊥], Xuming Zhang[§], Leo Lai Chan[†,⊥], Paul K. S. Lam[⊥], Paul K. Chu[§], Kwok-Yin Wong[∥], Mengsu Yang[*†,‡,⊥]

[†]Department of Biomedical Sciences, City University of Hong Kong, 83 Tat Chee Avenue, Kowloon, Hong Kong

[‡]Key Laboratory of Biochip Technology, Shenzhen Biotech and Health Centre, City University of Hong Kong, Shenzhen, 518057, People's Republic of China

[⊥]State Key Laboratory in Marine Pollution, City University of Hong Kong, 83 Tat Chee Avenue, Kowloon, Hong Kong

[§]Department of Physics and Materials Science, City University of Hong Kong, 83 Tat Chee Avenue, Kowloon, Hong Kong

[∥]Department of Applied Biology and Chemical Technology, and the State Key Laboratory of Chirosciences, The Hong Kong Polytechnic University, Hung Hom, Kowloon, Hong Kong

Corresponding author:

[*]Mengsu Yang

Tel: (852) 34427797/Fax: (852) 34420552. E-mail: bhmyang@cityu.edu.hk

Number of pages: 6

Number of figures: 6

Number of tables: 0

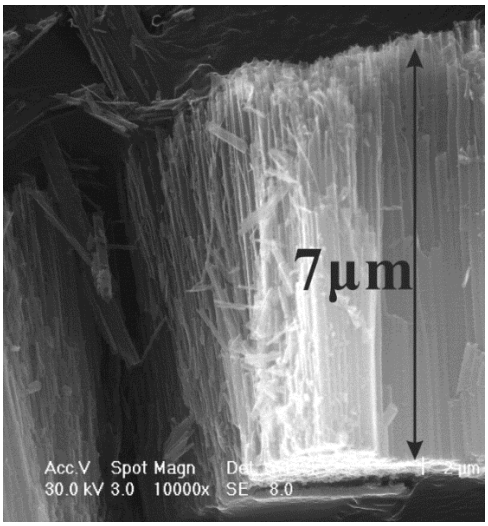

Figure S1. FE-SEM of the side-view image morphology of of TiO_2 NTAs.

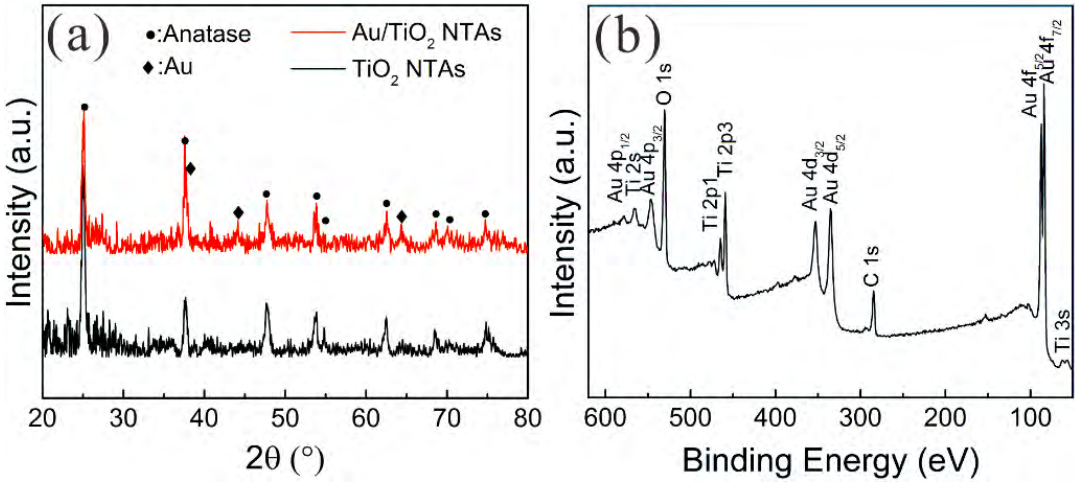

Figure S2. (a) XRD patterns of TiO_2 NTAs (black) and TiO_2/Au NTAs (red). (b) XPS surface scan spectrum of TiO_2/Au NTAs.

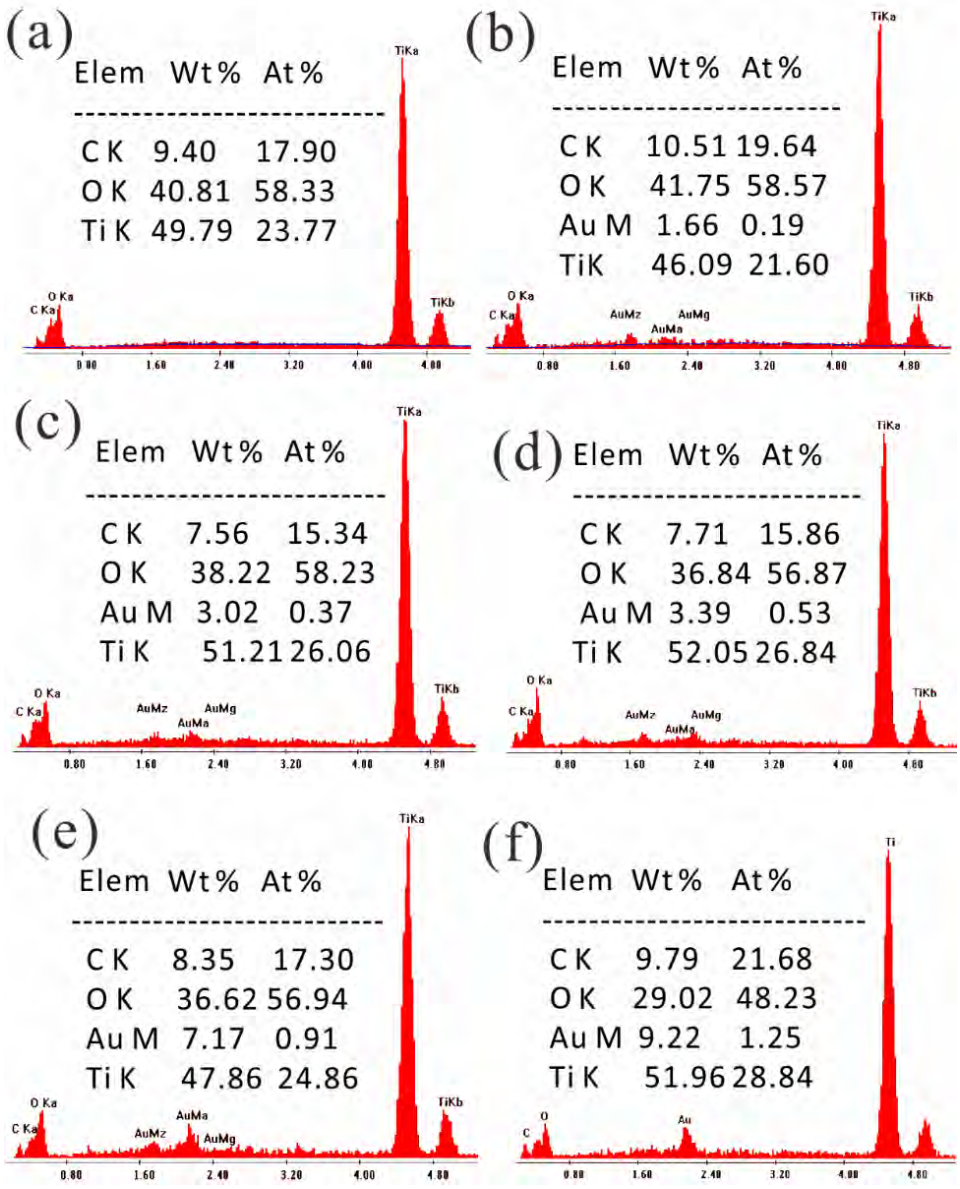

Figure S3. EDX spectra of TiO_2 NTAs (a) and TiO_2/Au NTAs (b-f) with different amount of Au NPs loading, respectively.

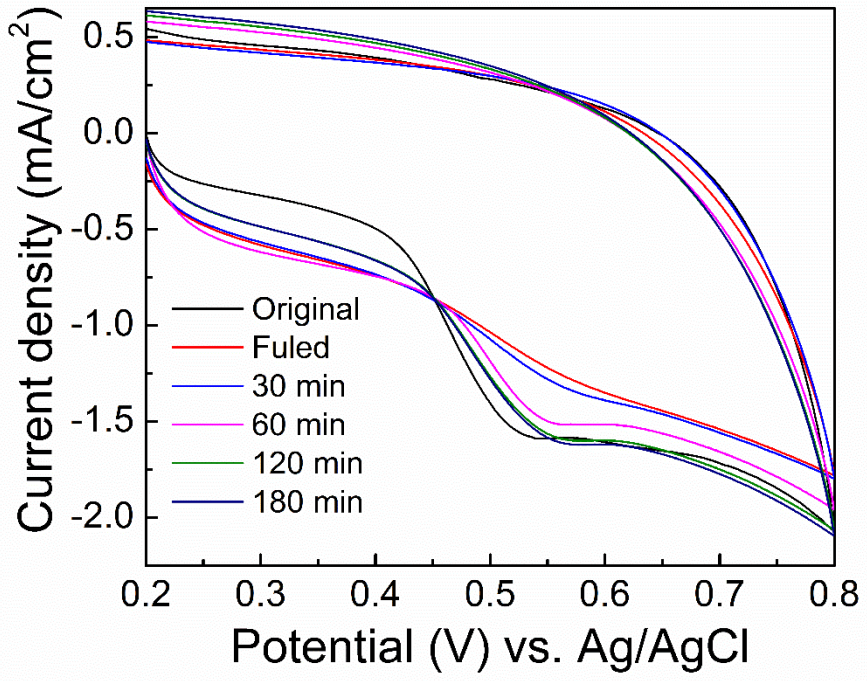

Figure S4. Cyclic voltammograms of 0.1 mM BPA in a 0.1 M PBS (pH 7.4) obtained at an original, fouled obtained at TiO_2/Au-3 NTAs electrode, and after UV light irradiation of the fouled TiO_2/Au-3 NTAs with 30-180 min, respectively. Scanning rate: 100 mV·s^{-1}.

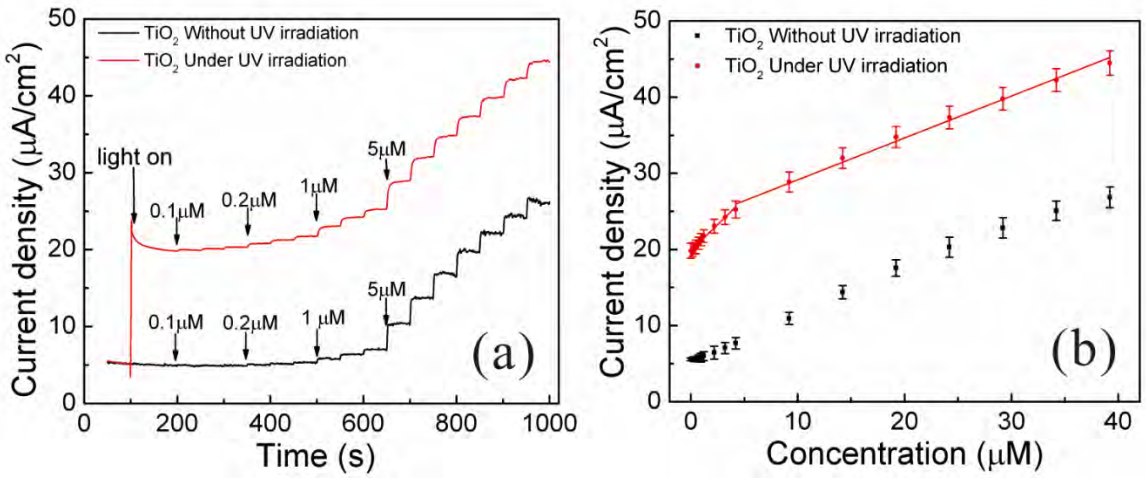

Figure S5. (a) Current–time recording obtained at TiO_2 electrode with successive addition of 0.1 μM -38.9 μM BPA into a stirred 0.1 M PBS (pH = 7.4) at an applied potential of 530 mV with/without UV irradiation, respectively. (b) The calibration curve of the respond currents versus concentrations of BPA with/without UV irradiation. The error bars represent the respond current of three independent experiments.

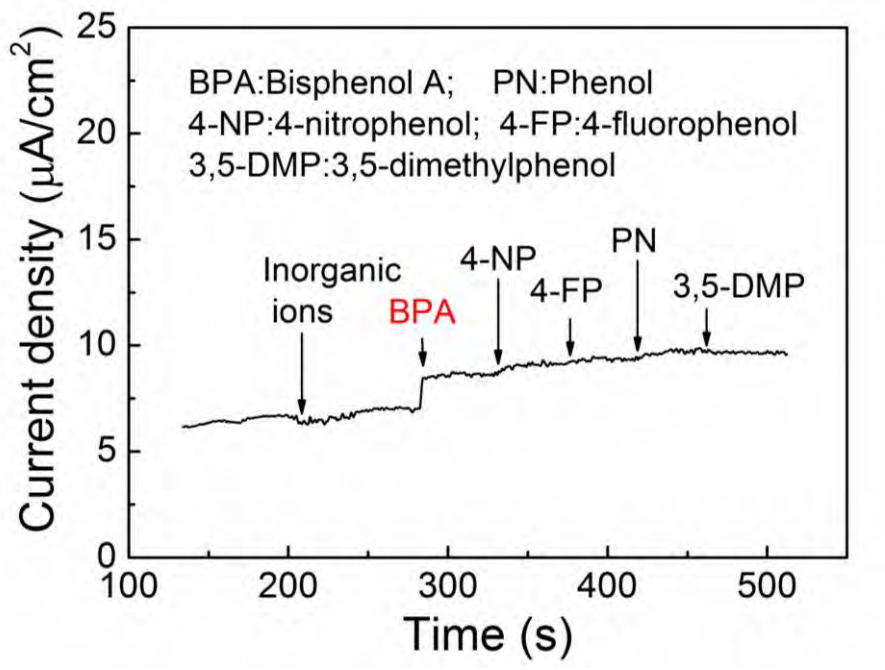

Figure S6. Current–time recording obtained at TiO_2/Au-3 NTAs electrode with addition of 100 μM inorganic ions (Na^+, K^+ Zn^{2+}, Ca^{2+}, Fe^{3+}, Cu^{2+}, SO_4^{2-}, NO_3^-, Cl^-, CO_3^-), 1.0 μM BPA, 20 μM 4-NP, 20 μM 4-FP, 20 μM PN and 20 μM 3, 5-DMP into a stirred 0.1 M PBS (pH = 7.4) at an applied potential of 530 mV, successively.